Challenge Journal of Concrete Research Letters

Research Article

The impact of openings on ferrocement I-beams: a study on metallic and non-metallic mesh reinforcement

Ghada Mousa Hekal [a,*], Ayman Magdy Moawad Elshaboury [b], Yousry B. I. Shaheen [a]

[a] *Department of Civil Engineering, Menoufia University, Shebin ElKoum, Menofia, Egypt*
[b] *Department of Construction, Higher Institute of Engineering and Technology, Beheira, Egypt*

ABSTRACT

The primary objective of this investigation is to assess the influence of openings on the structural performance of ferrocement I-beams, incorporating diverse metallic and non-metallic mesh reinforcements. Sixteen beams underwent testing utilizing a four-point loading system until failure, categorized into four groups based on the type of mesh reinforcement. Each group comprised a control I-beam without openings and three additional beams featuring one, two, and three openings, respectively. To ensure consistent reinforcement weight, the four groups were reinforced with three layers of welded steel meshes, two layers of expanded metal meshes, two layers of Tensar meshes, and eight layers of Gavazzi meshes. Comparative analysis of the experimental outcomes was conducted with finite element models utilizing Abaqus. Therefore, there was good agreement between the experimental and numerical results. The findings showed that beams with no openings, one, and two openings reinforced with Gavazzi meshes had the highest ultimate load compared to other tested beams, while beams with three openings, those reinforced with expanded metal meshes had the greatest ultimate loads. Placing three openings in beams, with dimensions of 100×50 mm (two of these openings are approximately 10 cm apart from each edge while the third opening is located at mid-span), reduced the load-to-weight ratio by about 20.7%, 12.9%, 8.2%, and 23.8% for welded beams, expanded beams, Tensar beams, and Gavazzi beams, respectively, compared to the beams with no openings.

ARTICLE INFO

Article history:
Received 14 September 2023
Revised 7 November 2023
Accepted 28 November 2023

Keywords:
Ferrocement
I-beams
Openings
Metallic meshes
Non-metallic meshes

1. Introduction

Ferrocement, a composite material reinforced with wire meshes, has gained attention due to its strength, serviceability, and durability as mentioned in ACI 549R (1997) and ACI 5492R (2004). This material consists of a mortar matrix with multiple layers of steel mesh reinforcement embedded within it (Shaheen et al. 2023a). It can be formed into various shapes using machinery, making it cost-effective and versatile. Ferrocement is durable, lightweight, fire-resistant, and environmentally stable as stated in a previous study conducted by Naaman (2000). Suresh (2004), and Austriaco (2006) argued that ferrocement consistent distribution of reinforcing wire meshes has made it an attractive option for pre-fabrication and construction development. The mesh can be produced from metallic or other appropriate materials (Shaheen et al. 2022a).

Several studies conducted by different authors such as Ankit et al. (2017), Shaheen et al. (2016, 2020, 2021, 2023b), Rameshkumar et al. (2022), Salman et al. (2018), Shaaban et al. (2018), Sumadi and Ramli (2008), International Ferrocement Society (2001), investigated the mechanical properties of ferrocement, including its compressive and flexural strength, as well as ductility behavior. Acma and Mariano (2014) examined ferrocement I-beams reinforced with two to six welded wire meshes and found that while the flexural strength was

* *Corresponding author*. Tel.: +02-010-698-560-09 ; E-mail address: gahda.mousa@sh-eng.menofia.edu.eg (G. M. Hekal)
ISSN: 2548-0928 / DOI: https://doi.org/10.20528/cjcrl.2024.02.001

satisfactory, the beams did not exhibit the required ductility behavior of reinforced concrete beams. Acma et al. (2015) conducted another study on ferrocement I-beams, using eight layers of welded wire mesh to reinforce C-beams. They found that the load increased with an increase in the number of welded wire mesh reinforcement layers in the flange area.

ChandraSekharRao et al. (2012) conducted an investigation on the behavior and durability of cored precast ferrocement beams with box section. They cast and tested eight box beams under a four-point bending setup, with the number of wire mesh layers as a variable parameter. The study found that the reduction in flexural strength due to vacancies was smaller than the reduction in weight, and the post-ductility increased by increasing the layer number, leading to an improvement in moment-curvature response of the cored specimens under flexural loading.

Shaheen et al. (2022b) conducted an experimental investigation on ferrocement I-beams featuring various metallic and non-metallic mesh reinforcements. 8 beams were cast, cured, and subjected to testing using a four-point bending system, with the beams categorized into two groups depending on the type of reinforcement employed. The beams reinforced with welded steel mesh exhibited superior ultimate loads, deflection, ductility ratio, and energy absorption in comparison to those reinforced with Tensar mesh. The introduction of three openings to 100×50 mm beams resulted in a reduction of the load-to-weight ratio by 20.7% and 8.2% for welded steel mesh-reinforced and Tensar mesh-reinforced beams, respectively.

This study aims to build upon previous research carried out by Shaheen et al. (2022b) by conducting a more comprehensive experimental program on ferrocement I-beams with openings, using various types of meshes for reinforcement. Ferrocement I-beams exhibit versatility in construction engineering with potential applications spanning various domains. Their high strength-to-weight ratio makes them suitable for small to medium-span bridges, marine structures like docks and piers, and building elements such as floors and roofs. Additionally, ferrocement I-beams can be employed in retaining walls, precast elements for controlled manufacturing conditions, water tanks due to their crack resistance, and infrastructure rehabilitation projects. Their lightweight nature makes them advantageous in seismic-prone regions and agricultural structures, while their corrosion resistance deems them fit for pipeline support structures. The goal is to provide further insight into the behavior of ferrocement I-beams with openings. Additionally, a finite element analysis will be conducted on all tested beams to gain a deeper understanding of their behavior. Hoping that this research will be a valuable addition to the existing literature on ferrocement and its applications.

2. Experimental Program

The authors aimed to expand on their previous research (Shaheen et al. 2022b) by conducting a more extensive experimental program, using additional ferrocement I-beams reinforced with various types of metal and non-metal meshes. The previous research referred to in this paper utilized eight ferrocement I-beams, which were divided into two groups based on the type of reinforcing mesh used, as listed in Table 1. In this study, an additional eight beams reinforced were added to the current study. These new beams were also categorized into two sets based on the type of the used reinforcing, as described in Table 1.

Table 1. Details of the tested beams (Shaheen et al. 2022b).

Group No.	Code of the beam	Meshes used	No. of openings	Volume fraction %
A	W0 control	Welded steel mesh arranged in triple layers	-	4.4
	W1		1	
	W2		2	
	W3		3	
B	T0 control	double layers of Tensar mesh (Type SS40)	-	1.3
	T1		1	
	T2		2	
	T3		3	
C	E0 control	double layers of expanded metal mesh	-	1.0
	E1		1	
	E2		2	
	E3		3	
D	G0 control	Eight-layer Gavazzi mesh (Type 0133-A)	-	4.6
	G1		1	
	G2		2	
	G3		3	

The formulation of the mortar mix in this study followed the same procedure as outlined in the prior investigation conducted by Shaheen et al. (2022b). The mortar mix included Blast furnace Cement, sand, silica fume, fly ash, water, Polypropylene mesh e300, and superplasticizer. Silica fume was used in conjunction with fly ash to achieve better strength with less cement, as demonstrated by Pathak (2020). Similarly, Safiuddin and Zain (2005) concluded that fly ash and silica fume together improved the fresh and hardened properties of concrete. Silica fume improved the permeability of concrete, while fly ash improved its strength over time. As shown in Fig. 1, Group C was reinforced with expanded metal mesh, while group D was reinforced with Gavazzi mesh. Tables 2 and 3 provide the technical specifications and mechanical properties of the expanded metal and Gavazzi meshes, respectively according to the manufacturer.

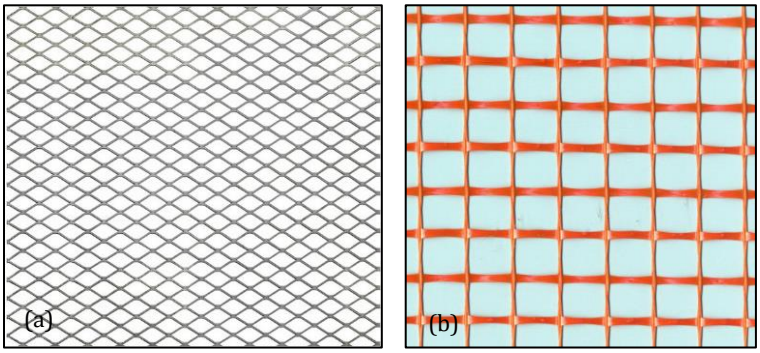

Fig. 1. The meshes applied to groups C and D: (a) Expanded metal mesh; (b) Gavazzi mesh.

Table 2. Expanded metal mesh – technical details and material properties.

Product name	Expanded metal mesh plaster wire mesh
Sheet size	1 m × 7 m
Weight	730 gm/m^2
Diamond size	16 mm × 31 mm
Dimensions of strand	1.25mm × 1.5mm
Proof Stress (N/mm^2)	199
Proof Strain (×10^{-3})	9.7
Ultimate Strength (N/mm^2)	320
Ultimate Strain (×10^{-3})	59.2

Table 3. Gavazzi mesh – technical details and material properties.

Product name	Gavazzi 0133-A	
Mesh openings	Approx. 12.5 mm × 11.5 mm	
Weight	120 gm/m^2 ± 5%	
Composition	Fiberglass approx. 82 %	
	Alkali-resistant finish approx. 18 %	
Resistance to tensile strength	Breaking strength	Elongation
	Warp approx. 1650 N/5 cm	5 % ± 1
	Weft approx. 2000 N/5 cm	5 % ± 1

The dimensions of the tested beams were identical to those of the previous study referenced in. The beams' fixed dimensions were as follows: length of 2200 mm, breadth of 200 mm, flange thickness of 40 mm, height of 170 mm, and web thickness of 30 mm, resulting in a total height of 250 mm for each specimen. The beams were loaded under a four-point load setup until failure, with 2000 mm between the two supports and 660 mm between the two loads. The choice of a four-point loading test is motivated by the suitability of the flexural test for assessing the strength of brittle materials, as it subjects the material to a pure bending load. This type of loading test holds particular significance in the examination of brittle materials, where the quantity and severity of flaws exposed to maximum stress directly influence flexural strength and crack initiation. In comparison to the three-point bending flexural test, the four-point loading test eliminates shear forces in the area between the two loading supports. Additionally, the utilization of a four-point loading test serves the purpose of evaluating how

much the mesh contributes to the manifestation of noticeable deformation before failure. Fig. 2 illustrates the sizes of the tested beams, while Fig. 3 shows the mesh pattern used during the production of the beams and up to the completion of casting.

The two primary factors examined were the type of meshes used and the number of openings in the web of the beam. The beams were intentionally weakened in the shear and moment zones by introducing openings. This was done to investigate the impact of these openings on the behavior of ferrocement I-beams reinforced with various types of metallic and non-metallic meshes. On the opposite side, the opening area was chosen to be small enough not to interfere with the beam's effectiveness while still allowing the necessary wires to pass-through.

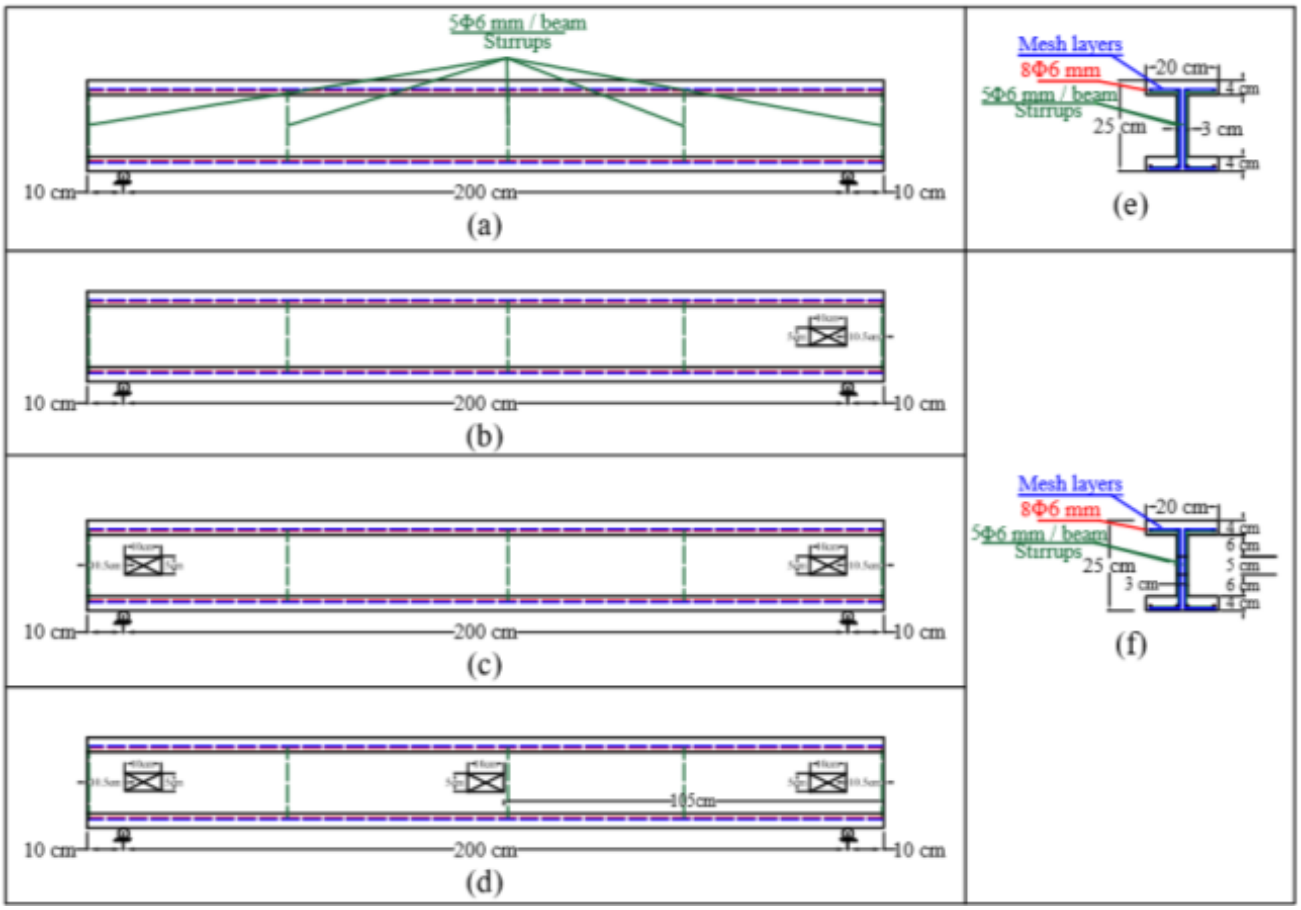

Fig. 2. Geometric **s**pecifications of **e**xamined beams and openings:
(a) Control beam; (b) Beams with one opening; (c) Beams with two openings; (d) Beams with three openings; (e) Side view of control beam; (f) Side view of beams with openings.

Fig. 3. The configuration of meshes employed in the preparation process:
(a) Beams featuring expanded metal mesh reinforcement; (b) Beams reinforced with Gavazzi mesh.

Throughout the testing procedure, the recorded data included the vertical displacement plotted against the applied load. The testing apparatus comprised loading cells, a control station, and a testing frame. Incremental loadings of 5.0 to 20 kN were systematically applied to each specimen. At each stage of loading, meticulous measurements of cracking patterns and deformation values were conducted. The experimental program took place in the laboratory of properties and testing materials at the Faculty of Engineering, Menoufia University, Egypt. The mixing method, curing conditions, and testing techniques employed mirrored those utilized in a previous study by the same authors.

3. Test Set-up and Instrumentation

Following a 28-day period, the beams were coated with white to facilitate the identification of cracks. For strain measurement against load, four demec points were strategically positioned on both the upper and lower flanges of the beam's mid-span on one side, as illustrated in Fig. 4. The measurements were then multiplied by the gauge coefficient of the mechanical gauge in use to estimate the strain values, and the dial gauge values at each load increment were recorded to calculate the beam deflection.

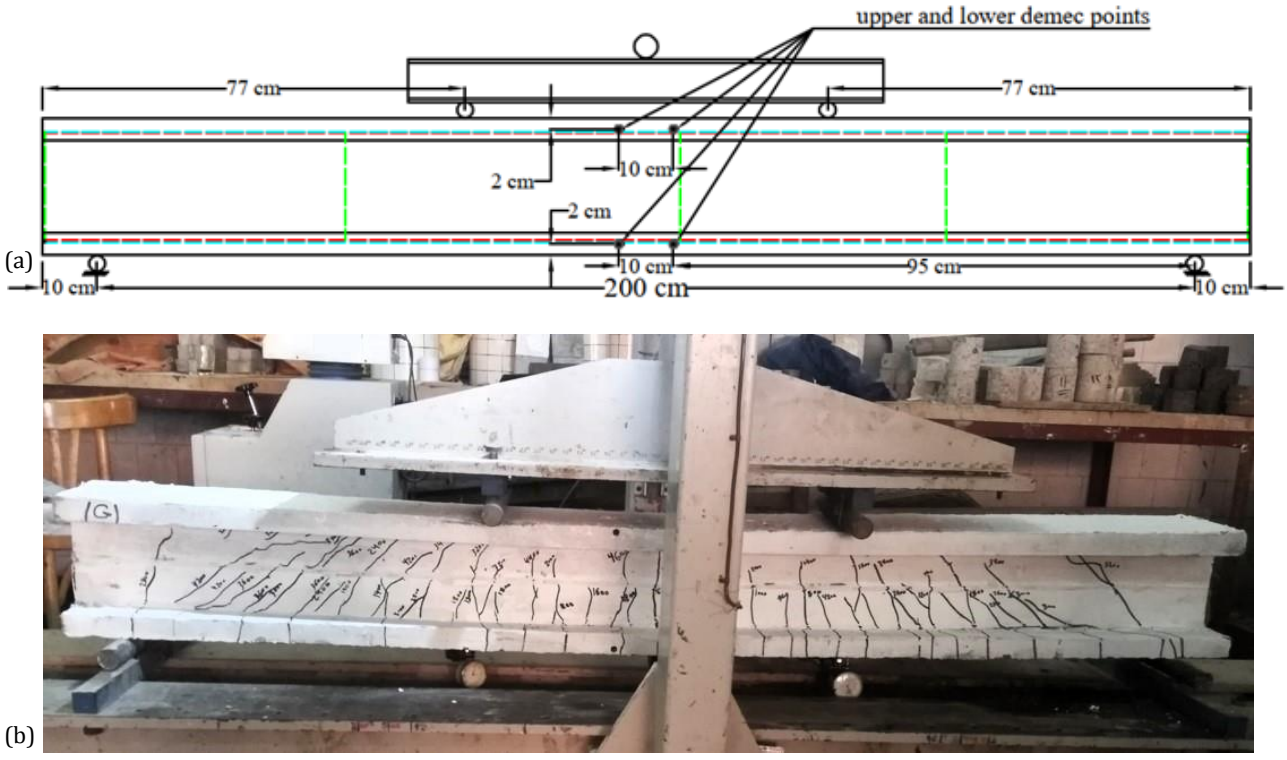

Fig. 4. Test setup: (a) Locations of the applied loads, and placement of demec points on the tested specimen; (b) Beam G0 under loading.

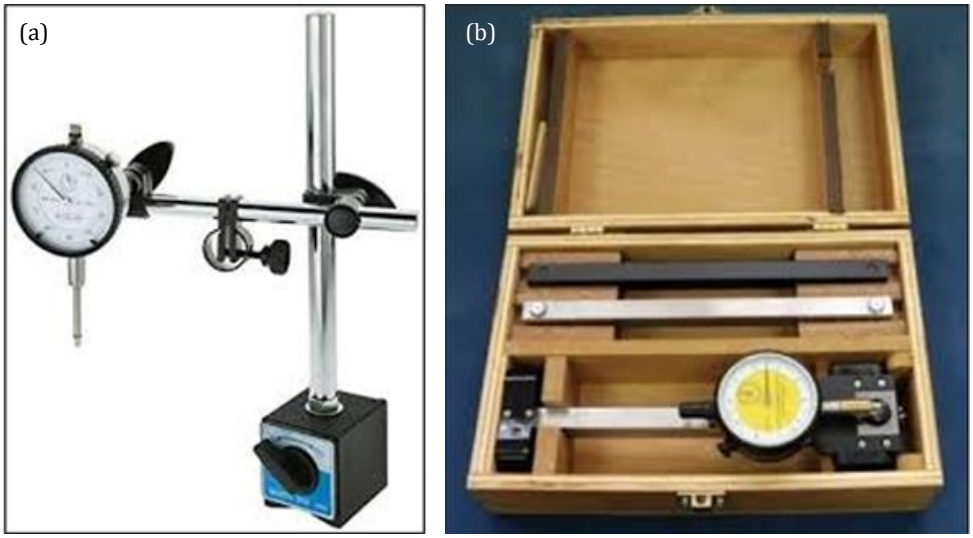

Fig. 5. Dial and deflection gauges used: (a) Dial gauge; (b) Strain gauge.

The specimen was positioned at the center of the testing apparatus, maintaining a uniform distance equals 2000 mm between the specimen supports. As depicted in Fig. 4, the applied loads were situated 770 mm away from each of the beam's ends. Fig. 5 displays the deflection and dial gauges utilized in the test

4. Finite Element Model

To validate the obtained findings and gain a better understanding of the performance of I-shaped ferrocement beams incorporating web perforations, finite element models were developed using Abaqus 6.14, in addition to experimental investigations. For this purpose, a 3D finite element model was created using Abaqus to study the nonlinear material and geometric responses of concrete, steel bars, and reinforced meshes.

4.1. Mesh size and element description

The brick element (C3D8R) shown in Fig. 6 was used to model the ferrocement I-beams. In contrast, the T3D2 element shown in Fig. 7, which is a three-dimensional line element with two nodes, was employed to simulate the steel bars, welded metal mesh, expanded metal mesh, and Gavazzi mesh. These elements are typically used in continuum elements, particularly in concrete members according to Abaqus user's guide (2014). In a recent article, Hekal et al. (2023) have recommended the use of C3D8R and T3D2 elements for beam modeling. On the other hand, to ensure precise simulation of the Tensar mesh, the shell element S4R depicted in Fig. 8 was utilized. The S4R element was chosen specifically to accurately represent the shape of the Tensar mesh.

Additionally, the models were partitioned into elements of diverse sizes, striking a balance between swift computation and precise analysis. The mesh dimensions used for each model were 10, 15, and 20 mm. Fine elements were strategically concentrated in the central loading region of the beam, as illustrated in Fig. 9. Simultaneously, coarse elements were employed near the edges of the beam. The reason for refining the element size in the middle is attributed to the significance of this area as the load impact zone and the location where deformation values were measured during the practical experiment.

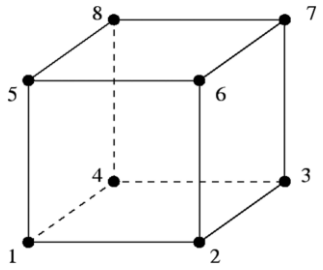

Fig. 6. 8-node 3-D solid (brick) element.

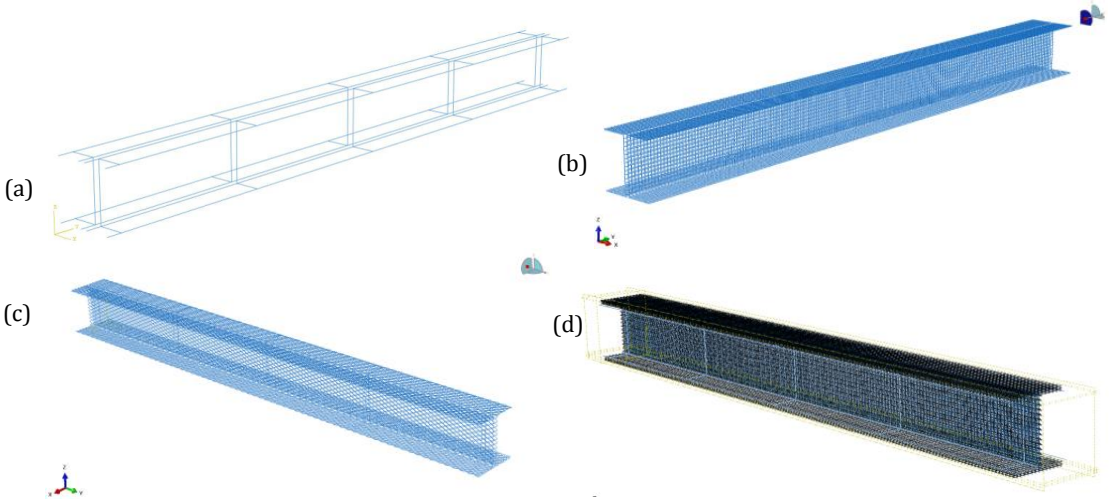

Fig. 7. Modeling of steel bars and reinforcing meshes using truss element: (a) Modeling of steel bars; (b) Modeling of welded metal meshes; (c) Modeling of expanded steel meshes; (d) Modeling of Gavazzi mesh.

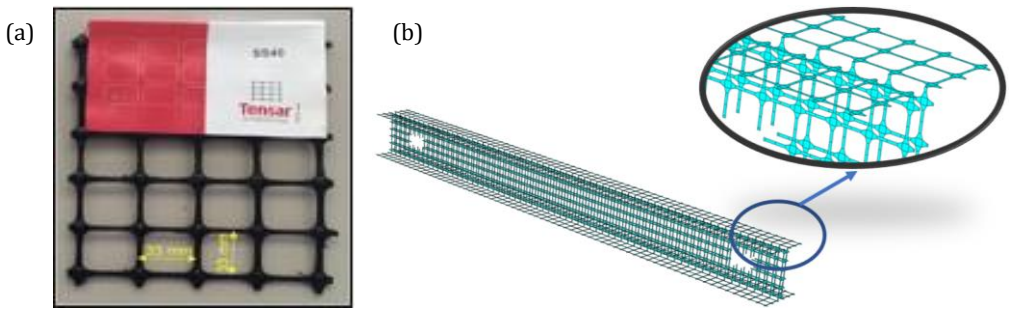

Fig. 8. Modeling of Tensar mesh using shell element:
(a) The real shape of Tensar meshes; (b) The modeling of Tensar using shell element.

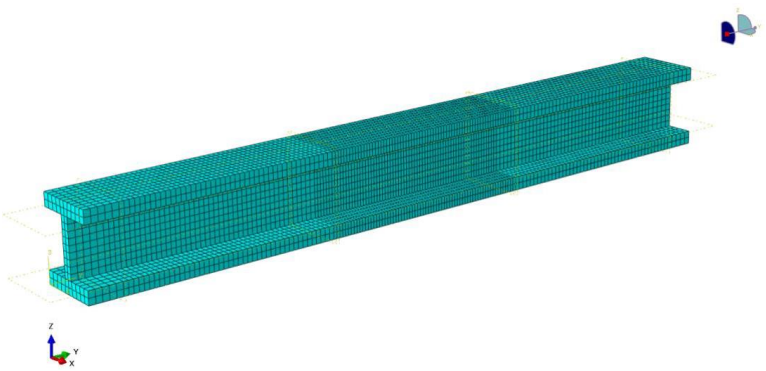

Fig. 9. Mesh representation of the concrete component.

4.2. Modeling of materials

Despite providing material characteristics for all elements, acquiring high-quality material information can be challenging, especially for more intricate material models like those involving material damage properties. The precision and comprehensiveness of pertinent data significantly influence the credibility and validity of the results.

To model the ferrocement I-beams, three different material models from Abaqus were used according to Abaqus User's Guide (2014). These include the concrete-damaged plasticity and the elastic-plastic models.

4.2.1. Concrete damaged plasticity model (CDP)

The Abaqus CDP model was chosen for the concrete material representation. This model incorporates the principles of isotropic damage elasticity, combined with isotropic compression and tensile plasticity, to simulate the inelastic behavior of concrete.

As illustrated in Fig. 10, the CDP model is used to indicate the uniaxial tension and compression behavior of concrete. When failure stresses are reached in the concrete, they are transformed into micro cracks in the concrete blocks. After the point of failure stress in concrete, the stress-strain behavior is influenced by the softening characteristic, depicted in Fig. 10(a). The response to uniaxial compression is linear until the initiation of yield (F_{cu}). Concrete exhibits stress hardening, succeeded by strain softening after attaining the ultimate stress (F_{cu}) within the plastic zone, as illustrated in Fig. 10(b). Consequently, concrete stresses dictate the unloading process from any given point on the strain curve.

$$f_t = E_c\,(\varepsilon_t - \varepsilon_t^{pl})\,(1 - dt) \tag{1}$$

$$f_c = E_c\,(\varepsilon_c - \varepsilon_c^{pl})\,(1 - dc) \tag{2}$$

where E_c is the modulus of elasticity of concrete. Then, the effective tensile and compressive cohesion stresses of concrete are estimated as:

$$\dot{f_c} = \frac{f_c}{(1-dc)} = E_c\left(\varepsilon_c - \varepsilon_c^{pl}\right) \tag{3}$$

$$\dot{f_t} = \frac{f_t}{(1-dt)} = E_c\left(\varepsilon_t - \varepsilon_t^{pl}\right) \tag{4}$$

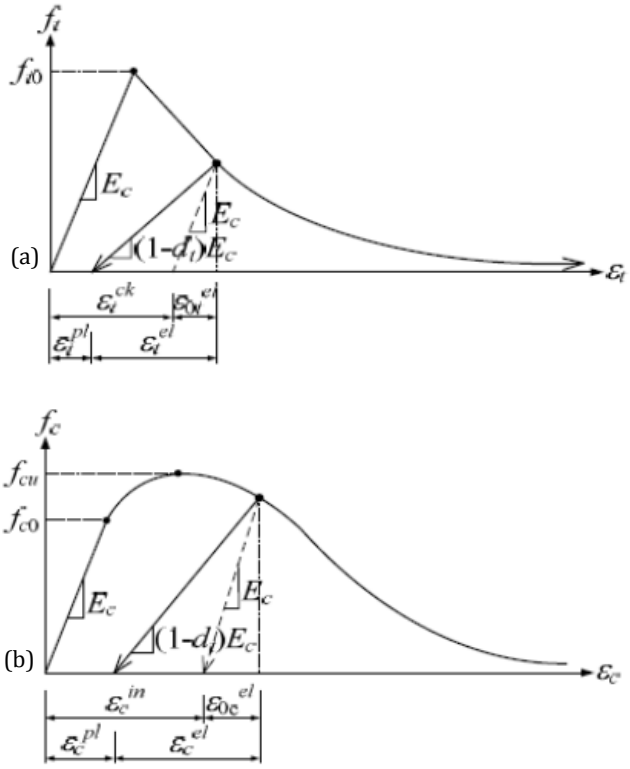

Fig. 10. Concrete damage plasticity behavior: (a) Tensile behavior associated with tension stiffening; (b) Compressive behavior associated with compression hardening.

The behavior of reinforced concrete after failure is illustrated by the post-failure stress, which is influenced by cracking strains ε_t^{ck} and ε_c^{ck}. These strains are characterized as the total strain minus the elastic strain associated with undamaged material, and tension stiffening information is presented concerning the cracking strains. In instances where unloading data is present, the programming automatically transforms cracking strain values into plastic strain values using predefined relationships:

$$\varepsilon_t^{pl} = \varepsilon_t^{ck} - \frac{d_t}{(1-d_t)} \times \frac{f_t}{E_c} \tag{5}$$

$$\varepsilon_c^{pl} = \varepsilon_c^{ck} - \frac{d_c}{(1-d_c)} \times \frac{f_c}{E_c} \tag{6}$$

Tables 4 and 5 list concrete elastic properties and CDP model parameters used in the analysis. The modulus of elasticity of concrete was determined according to the next formula:

$$E_c = 4400\sqrt{F_{cu}} \quad (\mathrm{N/mm^2}) \tag{7}$$

where, F_{cu} is the average compressive strength of the standard cubes at 28 days.

Table 4. Elastic characteristics of the concrete.

Parameter	Value
Density	2.2×10^{-9} N/mm^3
Modulus of elasticity (E_s)	26×10^3 MPa
Poisson's ratio (υ)	0.2

Table 5. Concrete damaged plasticity parameters.

Parameter	Value
Dilation angle	40°
Eccentricity	0.11
f_{b0}/f_{c0}	1.36
K	0.68
Viscosity parameter	0.00001

4.2.2. Elastic-plastic model

Steel bars as well as metal meshes were simulated using a linear elastic-plastic model, as depicted in Fig. 11. The linear behavior signifies the elastic phase up to the yield point, succeeded by the hardening phase representing the plastic stage up to the ultimate load. The mechanical properties of the steel bars, in accordance with E.S.S. 262 (2011), and the specification of the metal meshes used for modeling, as provided by the manufacturer, are detailed in Table 6.

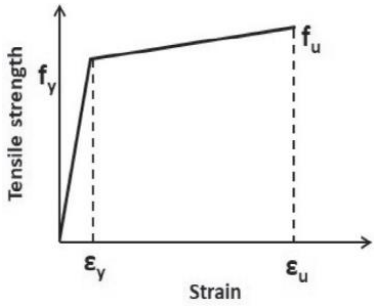

Fig. 11. The stress-strain curve for the steel.

As non-metal meshes exhibit brittle characteristics, and their stress-strain curves lack plastic deformation prior to abrupt failure, they were represented as elastic materials in the model. In Abaqus, the proof stress for each material was defined to determine the failure point during analysis. Table 7 presents the mechanical properties of the non-metal meshes utilized for modeling according to the manufacturer.

Table 6. Mechanical characteristics of steel bars and metal meshes.

Steel 24/35		Welded mesh		Expanded mesh	
Mass density, kg/m^3		Mass density, kg/m^3		Mass density, kg/m^3	
7859		7800		7800	
E, MPa	Poisson's ratio, υ	E, MPa	Poisson's ratio, υ	E, MPa	Poisson's ratio, υ
205×10^3	0.3	170×10^3	0.28	130×10^3	0.28
Stress, MPa	Plastic strain	Stress, MPa	Strain	Stress, MPa	Strain
240	0	413	0	199	0
350	0.0951	610	0.05763	320	0.0495

Table 7. Mechanical properties of non-metal meshes.

Tensar mesh		Gavazzi mesh	
Mass density, kg/m^3		Mass density, kg/m^3	
1590		1210	
E, MPa	100×10^3	E, MPa	80×10^3
Poisson ratio	0.3	Poisson ratio	0.3
Proof stress, MPa	198.43	Proof stress, MPa	325

4.3. Boundary conditions and load application

The supports of the ferrocement I-beam were restrained from translating in the YZ directions and rotating about the XZ plan at the two contact lines beneath the roller supports. Two line loads were applied to the ferrocement I-beam at a similar distance from the support line. The boundary conditions and loads are depicted in Fig. 12.

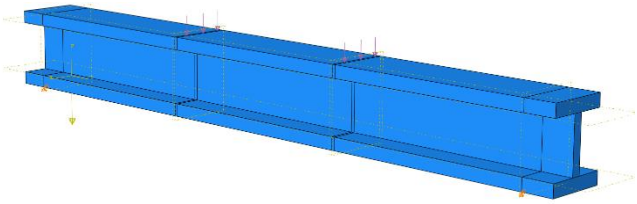

Fig. 12. Simply supported boundary conditions and load applied in the F.E. model.

4.4. Contact definition

The embedded element technique is employed to define an element or a cluster of elements embedded within a set of host elements. According to the Abaqus User's Guide (2014), this method utilizes the response of the host elements to constrain the translational degrees of freedom of the embedded nodes. It is particularly well-suited for modeling truss or beam elements embedded within a set of solid elements. This interaction type was chosen to model the interaction between the concrete beam and reinforced mesh. Fig. 13 depicts the resulting pattern of the beam after applying this interaction technique.

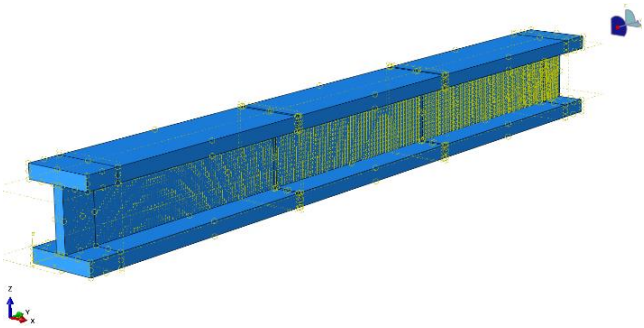

Fig. 13. The beam's pattern after the applying interaction.

5. Comparison of Experimental and Numerical Results

To validate the finite element model developed for this study, a comparison is made between the numerical and experimental results.

5.1. Initial crack loads, ultimate loads, and peak deflections of tested beams

Table 8 presents the findings of experimental and FE model for the initial crack loads, ultimate loads, and mid-span deflections of the tested beams. The results demonstrate that FE simulations yield accurate and compatible results when compared to experimental results. The average first crack load difference as a percentage is approximately 5.5%, while the average ultimate load difference is approximately 5%. Furthermore, the average difference in maximum deflections between the experimental and FE results is approximately 5.8%. Fig. 14 illustrates the relationships between the applied load and both experimental and FE first crack loads, ultimate loads, and maximum deflections of all tested beams.

As depicted in Fig. 14, Beam G0 demonstrated the highest ultimate load at 48.33 kN, while Beam T3 exhibited the lowest ultimate load at 34.45 kN. Additionally, Beam G0 recorded the maximum first cracking load of 14.50 kN, whereas Beam W3 had the minimum first cracking load of 9.59 kN.

Comparing beams with Gavazzi meshes to those with welded steel meshes, Gavazzi meshes exhibited a higher ultimate load by 3.8%, 8.6%, and 3.9% for beams without openings, one opening, and two openings, respectively. Furthermore, beams with Gavazzi meshes displayed a higher ultimate load compared to beams with expanded metal meshes by 9.2%, 10.1%, and 2.5% for beams without openings, one opening, and two openings, respectively.

In the comparison of non-metal meshes, Gavazzi meshes demonstrated a higher ultimate load than Tensar meshes by 23.2%, 21.3%, 15.6%, and 10.2% for beams without openings, one opening, two openings, and three openings, respectively. This outcome is likely attributed to the superior properties of Gavazzi meshes as non-metallic materials, enhancing the performance of the beams more effectively than other mesh types. Regarding the comparison between metal meshes used, beam W0 exhibited a higher deflection than beam E0 by 3.3%, while beams W1, W2, and W3 exhibited lower deflections than beams E1, E2, and E3 by 3.2%, 5.7%, and 11.3%, respectively. In addition, when comparing non-metal meshes used, beams G0, G1, G2, and G3 exhibited higher deflections than beams T0, T1, T2, and T3 by 5.2%, 3.3%, 9.5%, and 5.9%, respectively.

From Fig. 14, it was observed that the first crack load of beams T2 and T3 was higher than the first crack load of beams T0 and T1.

5.2. Ductility ratio

The ductility ratio, representing the relationship between the mid-span deflection at the ultimate load and that at the first crack load, was computed for each tested beam. The results are tabulated in Table 9, and a visual representation is depicted in Fig. 15. As shown in Fig. 15, for beams without openings and with one opening, those reinforced with welded metal mesh have a higher ductility ratio compared to their counterparts in other groups, while for beams with two and three openings, beams reinforced with expanded meshes have higher ductility ratios compared to the other beams with two and three openings. This may be due to the higher maximum deflection values of welded beams without openings and with one opening and beams reinforced with expanded

meshes with two and three openings, while the deflection at first crack loads of welded beams without openings and with one opening and beams reinforced with expanded meshes with two and three openings is close to the deflection at first crack loads of the other beams. In addition, as shown in Fig. 15, beam W0 had the highest ductility ratio among all the tested beams, while beam G3 obtained the lowest ductility ratio. This finding is supported by a previous study conducted by Shaaban et al. (2018) that showed that beams reinforced with Gavazzi meshes had the lowest ductility ratio when compared to beams reinforced with steel meshes. The results indicate that the FE simulations achieve accurate and consistent results when compared to the experimental results, with a mean difference of 2.2% between the investigational and FE ductility ratios.

Table 8. Comparative analysis of first crack loads, ultimate loads, and maximum deflection between experimental and finite element results.

Group name	Code of the beams	First crack load (kN)			Ultimate load (kN)			Maximum deflection (mm)		
		Experimental	F.E.	Difference (%)	Experimental	F.E.	Difference (%)	Experimental	F.E.	Difference (%)
A	W0	11.15	11.73	5.2	45.11	46.56	3.2	12.50	12.80	2.4
	W1	10.23	10.72	4.8	41.25	42.56	3.2	10.90	11.24	3.6
	W2	9.65	10.16	5.3	37.98	40.31	6.1	9.74	10.46	7.4
	W3	9.04	9.59	6.0	35.42	38.04	7.4	9..00	9.55	6.2
B	T0	10.96	11.54	5.3	36.97	39.24	6.1	6.75	7.28	7.8
	T1	10.74	11.20	4.3	36.19	38.11	5.3	6.64	7.20	8.5
	T2	13.13	13.94	6.2	34.52	36.22	4.9	5.81	6.24	7.4
	T3	12.58	13.26	5.4	33.6	34.45	2.5	5.68	5.92	4.3
C	E0	10.79	11.16	3.4	42.64	44.26	3.8	11.94	12.39	3.8
	E1	10.00	10.58	5.8	39.75	41.98	5.6	10.81	11.61	7.4
	E2	9.86	10.29	4.4	38.76	40.84	5.4	10.75	11.09	3.2
	E3	9.22	9.97	8.1	36.78	39.56	7.6	9.99	10.77	7.8
D	G0	14.02	14.50	3.4	46.88	48.33	3.1	7.28	7.66	5.3
	G1	13.08	13.87	6.0	44.98	46.24	2.8	7.01	7.44	6.1
	G2	11.76	12.56	6.8	39.68	41.88	5.5	6.34	6.83	7.6
	G3	10.63	11.39	7.2	35.39	37.97	7.3	6.00	6.27	4.5

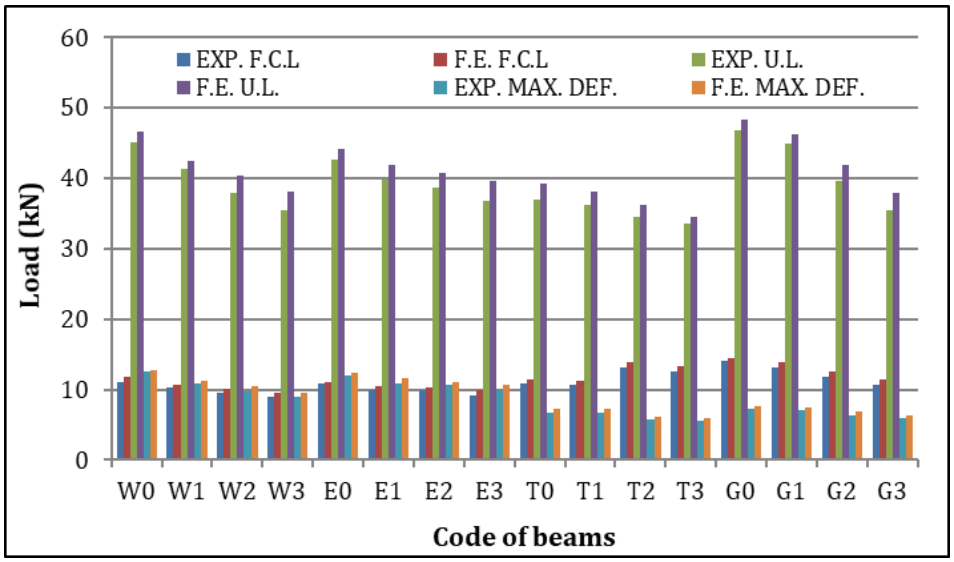

Fig. 14. The relation between the applied load and both experimental F.C.L., F.E. F.C.L., experimental U.L., F.E. U.L., experimental maximum deflection, and F.E. maximum deflection of all tested beams.

Table 9. Comparison between the experimental and F.E. results of ductility ratio, and load-to-weight ratio.

Group name	Code of the beams	Ductility ratio			Load-to-weight ratio (kg/kg)			Energy absorption (kN·mm)		
		Experimental	F.E.	Difference (%)	Experimental	F.E.	Difference (%)	Experimental	F.E.	Difference (%)
A	W0	10.86	11.26	3.6	55.05	56.82	3.2	303.2	320.5	5.7
	W1	9.96	10.26	2.9	50.51	52.10	3.1	238.9	255.2	6.8
	W2	9.49	9.36	1.4	46.65	49.51	6.1	197.4	224.9	13.9
	W3	8.83	8.64	2.2	43.64	46.88	7.4	169.0	192.7	14.1
B	T0	5.56	5.51	0.9	45.12	47.88	6.1	129.1	147.7	7.7
	T1	5.54	5.48	1.1	44.31	46.66	5.3	126.0	143.9	13.5
	T2	7.36	7.48	1.7	42.40	44.49	4.9	122.0	137.4	8.7
	T3	7.19	7.48	3.8	41.40	42.46	2.6	117.7	125.9	16.0
C	E0	10.71	10.64	0.6	52.04	54.01	3.8	272.4	293.5	14.4
	E1	10.33	9.91	4.3	48.67	51.40	5.6	229.7	260.7	14.2
	E2	10.02	9.86	1.6	47.61	50.16	5.4	221.7	241.1	12.6
	E3	9.82	9.51	3.3	45.32	48.75	7.6	196.0	227.4	6.9
D	G0	6.00	5.91	1.4	57.21	58.99	3.1	176.3	191.5	8.6
	G1	5.94	5.85	1.7	55.07	56.61	2.8	164.1	179.0	9.0
	G2	5.72	5.47	4.7	48.74	51.44	5.5	132.2	150.2	13.6
	G3	5.44	5.40	0.7	43.61	46.79	7.3	112.3	125.9	12.1

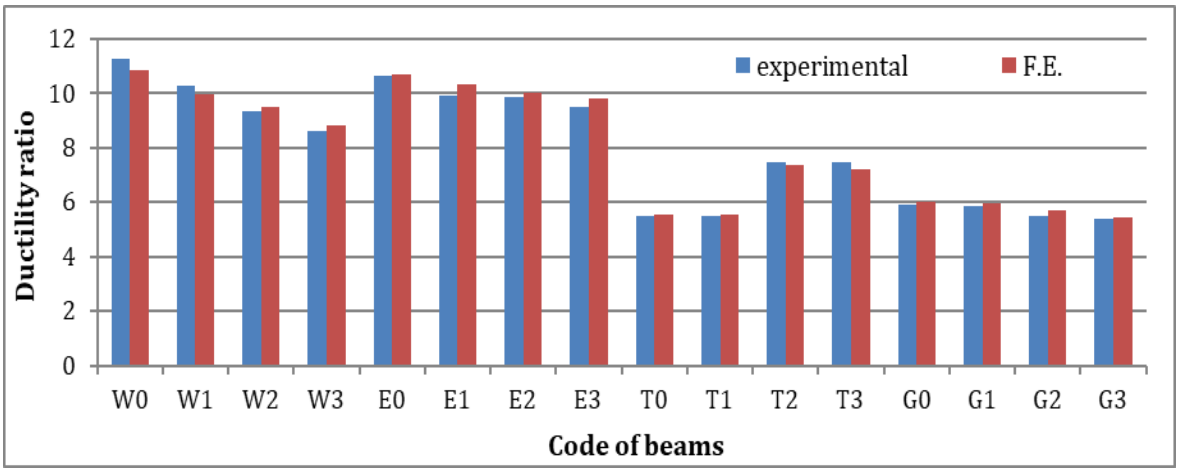

Fig. 15. Experimental and F.E. ductility ratio of all tested beams.

5.3. Load versus deflection relationships

Table 8 presents the ultimate load and maximum central deflection for each tested beam, while Figs. 16 to 20 depict the relationship between applied load and central deflection for each examined beam.

Analyzing the figures reveals that, for beams without openings, beam W0 exhibited a higher deflection than others, with a 3.3%, 75.9%, and 67.0% increase compared to beams E0, T0, and G0, respectively. Similarly, in beams with one opening, beam E1 had a higher deflection, with a 3.3%, 61.2%, and 56.1% increase compared to beams W1, T1, and G1, respectively. Additionally, in beams with two openings, beam E2 showed a higher deflection, with a 6.1%, 77.8%, and 62.5% increase compared to beams W2, T2, and G2, respectively. Finally, for beams with three openings, beam E3 had a higher deflection, with a 12.7%, 82.0%, and 71.9% increase compared to beams W3, T3, and G3, respectively.

Figure 17 highlights that within the 5 kN to 30 kN load range, the deflection of beams T2 and T3 is consistently lower than that of T0 and T1. This difference may be attributed to the fact that in T0 and T1, failure occurred primarily due to bending, leading to higher bending moment values and subsequently elevated deflection values. Conversely, in T2 and T3, stresses were distributed

around the openings in the shear zone, resulting in lower deflection values.

Comparing maximum deflection values, for welded steel meshes, beams W3, W2, and W1 had lower values than W0, with a decrease of 25.3%, 18.3%, and 12.2%, respectively. Similarly, for expanded metal meshes, beams E3, E2, and E1 had lower values than E0, with a decrease of 13.1%, 10.5%, and 6.3%, respectively. In the Tensar meshes group, beams T3, T2, and T1 had lower values than T0, with a decrease of 18.7%, 14.3%, and 1%, respectively. Finally, for the Gavazzi meshes group, beams G3, G2, and G1 had lower values than G0, with a decrease of 18.2%, 10.9%, and 2.9%, respectively.

In conclusion, the detailed analysis suggests that the configuration of openings, the specific arrangement of mesh types, and the distribution of stress in shear and bending zones play pivotal roles in determining the deflection behavior of the tested beams. This information is crucial for optimizing beam design and understanding the interplay between structural elements in real-world applications.

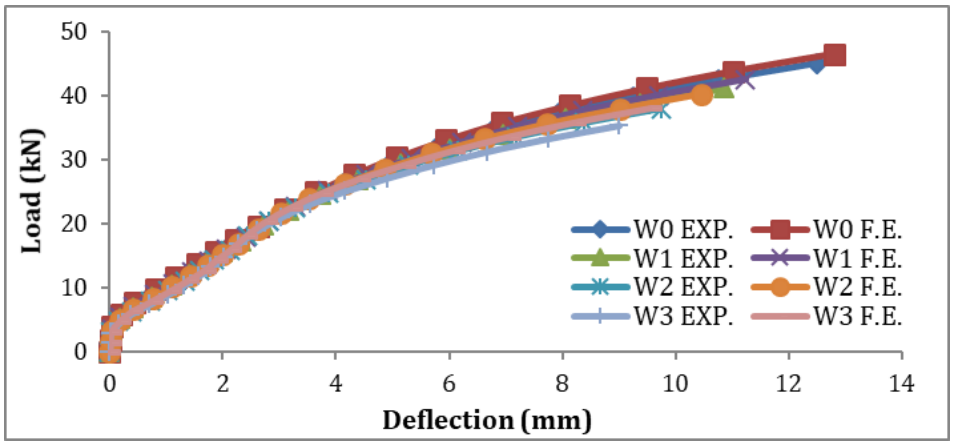

Fig. 16. Load-deflection curves of the group (A).

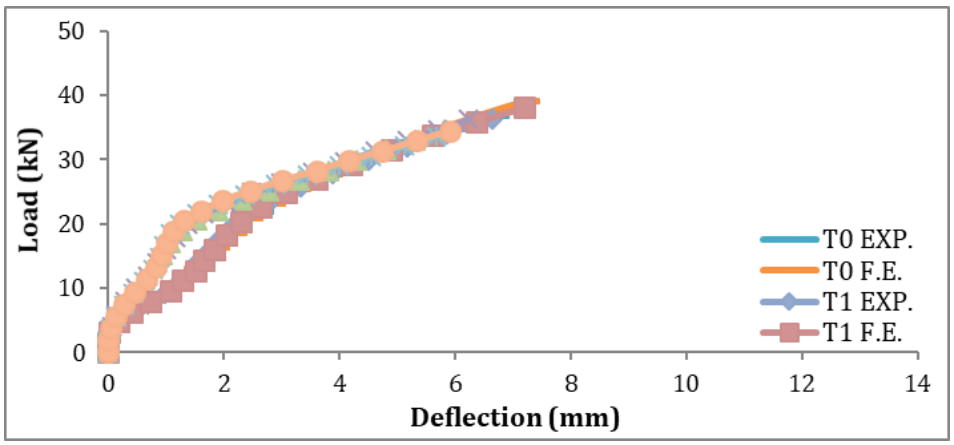

Fig. 17. Load-deflection curves of the group (B).

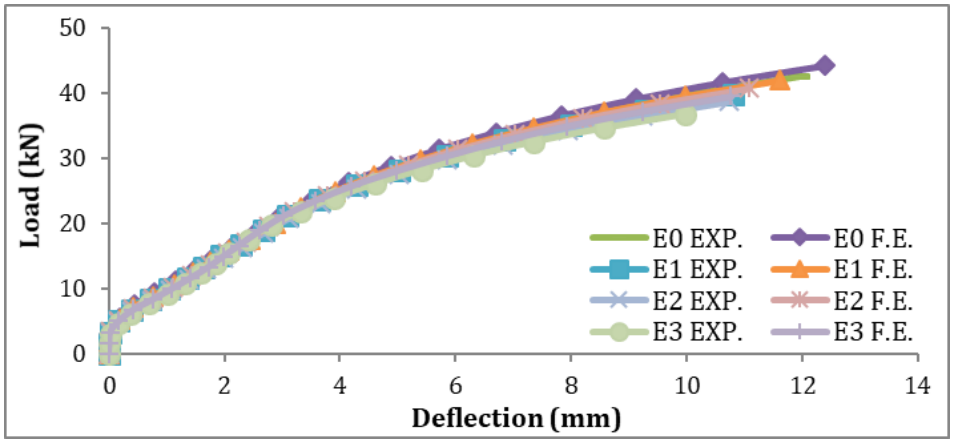

Fig. 18. Load-deflection curves of the group (C).

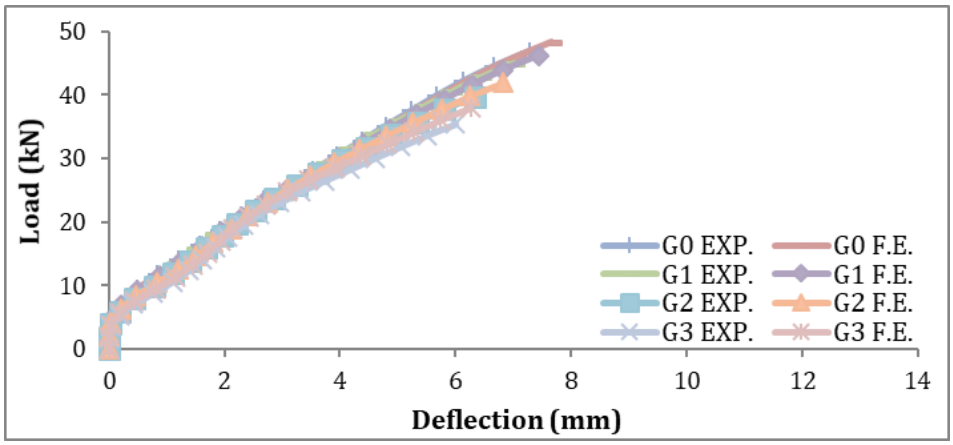

Fig. 19. Load-deflection curves of the group (D).

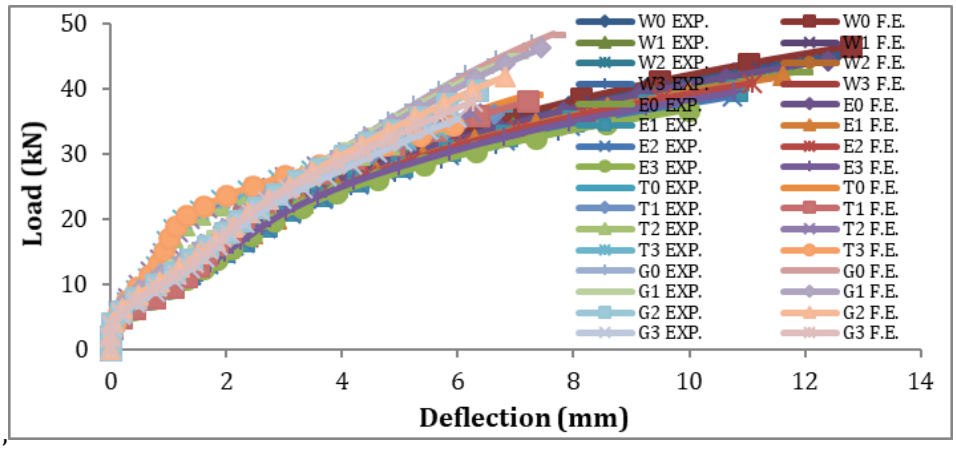

Fig. 20. Load-deflection curves of all tested beams.

5.4. Energy absorption

The quantity of energy absorbed by a beam is depicted by the area beneath its load-deflection curve. To compute this area, the load-deflection curve equation for each beam specimen was integrated using a computer program written in the BASIC language, outlined as follows:

$$\text{Ultimate load energy absorbed} = \int_0^{\Delta u} f(\Delta)\, d\Delta \qquad (8)$$

where $f(\Delta)$ represents the load defection curve equation.

The integration was performed from zero deflection to the mid-point deflection at the failure load, represented by the symbol u. The energy absorbed by each beam is listed in Table 9 and shown graphically in Fig. 21. From the figure, it can be observed that beam W0 absorbed the most energy among all the tested beams, while beam G3 absorbed the least. This is due to the large area beneath the load-deflection curve of beam W0 and the small area under the load-deflection curve of beam G3.

5.5. Load-to-weight ratio

To investigate the effect of the opening number on the performance of beams, the load-to-weight ratio was determined by dividing the ultimate load by the weight of the beams. The load-to-weight ratio values for all tested beams are presented in Table 9 and shown in Fig. 22. The results indicate that as the number of openings increases, the load-to-weight ratio decreases. Specifically, for welded, expanded metal, Tensar, and Gavazzi beams, placing three openings decreased the load-to-weight ratio by 17.5%, 9.7%, 11.3%, and 20.7%, respectively, compared to beams without openings. Placing two openings decreased the load-to-weight ratio by 12.9%, 7.1%, 7.1%, and 12.8%, respectively. Additionally, placing one opening in beams with dimensions of 100×50 mm reduced the load-to-weight ratio by 8.3%, 4.8%, 2.5%, and 4.0% for welded, expanded metal, Tensar, and Gavazzi beams, respectively, compared to beams with no openings. The reduction in load-to-weight ratios is proportional to the volume of openings in the beams.

5.6. Effect of openings on the performance of tested beams

When comparing various types of metal mesh, it was observed that the ultimate load in beams with three openings decreased by 18.3% for welded steel mesh beams and by 10.6% for expanded metal mesh beams, compared to beams without openings. In contrast, concerning non-metal meshes, the ultimate load in beams with three openings decreased by 21.4% for Gavazzi

mesh beams and by 12.2% for Tensar mesh beams compared to beams without openings.

Introducing three openings in beams with dimensions of 100×50 mm resulted in a reduction of maximum deflection by 28%, 16.3%, 15.9%, and 17.6% for welded beams, expanded beams, Tensar beams, and Gavazzi beams, respectively, compared to beams without openings. Furthermore, placing three openings in these beams reduced the ductility ratio by 23.3%, 10.6%, and 8.6% for welded beams, expanded beams, and Gavazzi beams, respectively. Energy absorption was also reduced by 39.9%, 22.5%, 14.8%, and 34.3% for welded beams, expanded beams, Tensar beams, and Gavazzi beams, respectively, when three openings were introduced in beams with dimensions of 100×50 mm, compared to beams without openings.

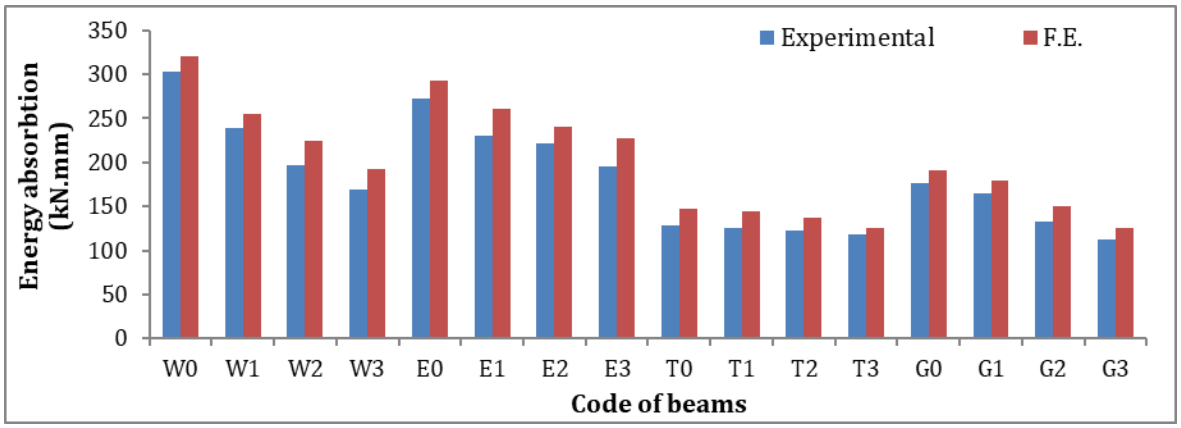

Fig. 21. The energy absorbed by all examined beams.

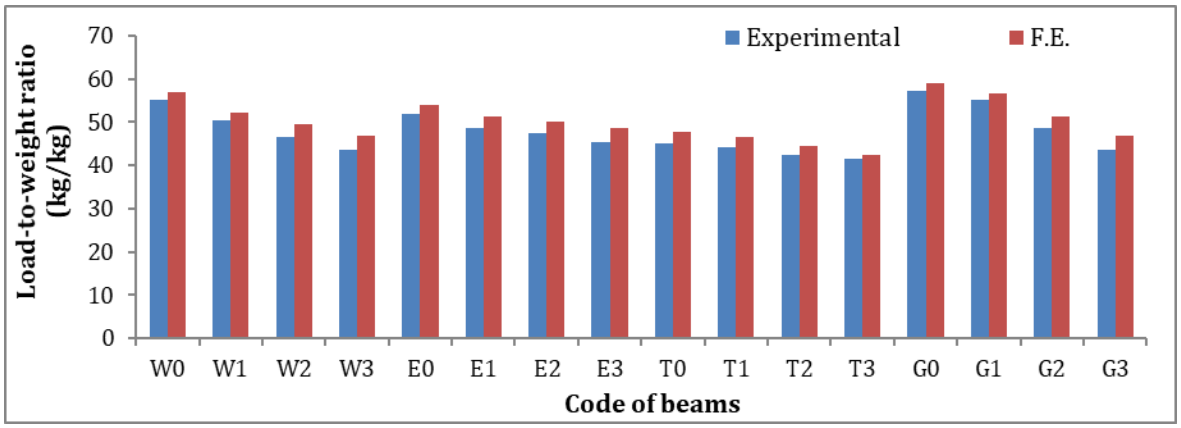

Fig. 22. Experimental and F.E. load-to-weight ratio of all tested beams.

5.7. Cracking patterns and mode of failure

The surface of the beams was inspected, and cracks were identified and marked. The initial crack load, crack propagation, and failure mode were determined for each beam. Flexural cracks appeared near the center of the beam and widened vertically as the load increased. New flexural cracks appeared rapidly and spread wider as the beam approached its failure load. Although most cracks did not reach the top surface of the beam, the crack at midspan grew vertically towards it. Fig. 23 illustrates the cracking shapes and mode of failure for all tested beams. The cracking patterns and mode of failure for beams with openings reinforced by welded steel meshes and expanded metal meshes appear to be a combination of shear and bending failure, with the greatest effect due to bending. In contrast, the cracking patterns and mode of failure for beams with openings reinforced by Tensar meshes and Gavazzi meshes appear to be mainly due to bending.

6. Conclusions

This paper investigates the impact of web openings on the structural behavior of ferrocement I-beams reinforced with metallic or non-metallic meshes. Sixteen beams were cast and tested to study their behavior under flexural loading. The tested beams were grouped into four groups based on the type of reinforcing mesh used, with each group consisting of four beams with the same reinforcement bars and meshes, but with different numbers of web openings.

Welded metal meshes and expanded steel meshes were used as reinforcing meshes for groups A and C, respectively, while Tensar meshes and Gavazzi meshes were used for groups B and D, respectively. To maintain a constant reinforcement weight, the four groups were reinforced with three layers of welded steel meshes, two layers of expanded metal meshes, two layers of Tensar meshes, and eight layers of Gavazzi meshes.

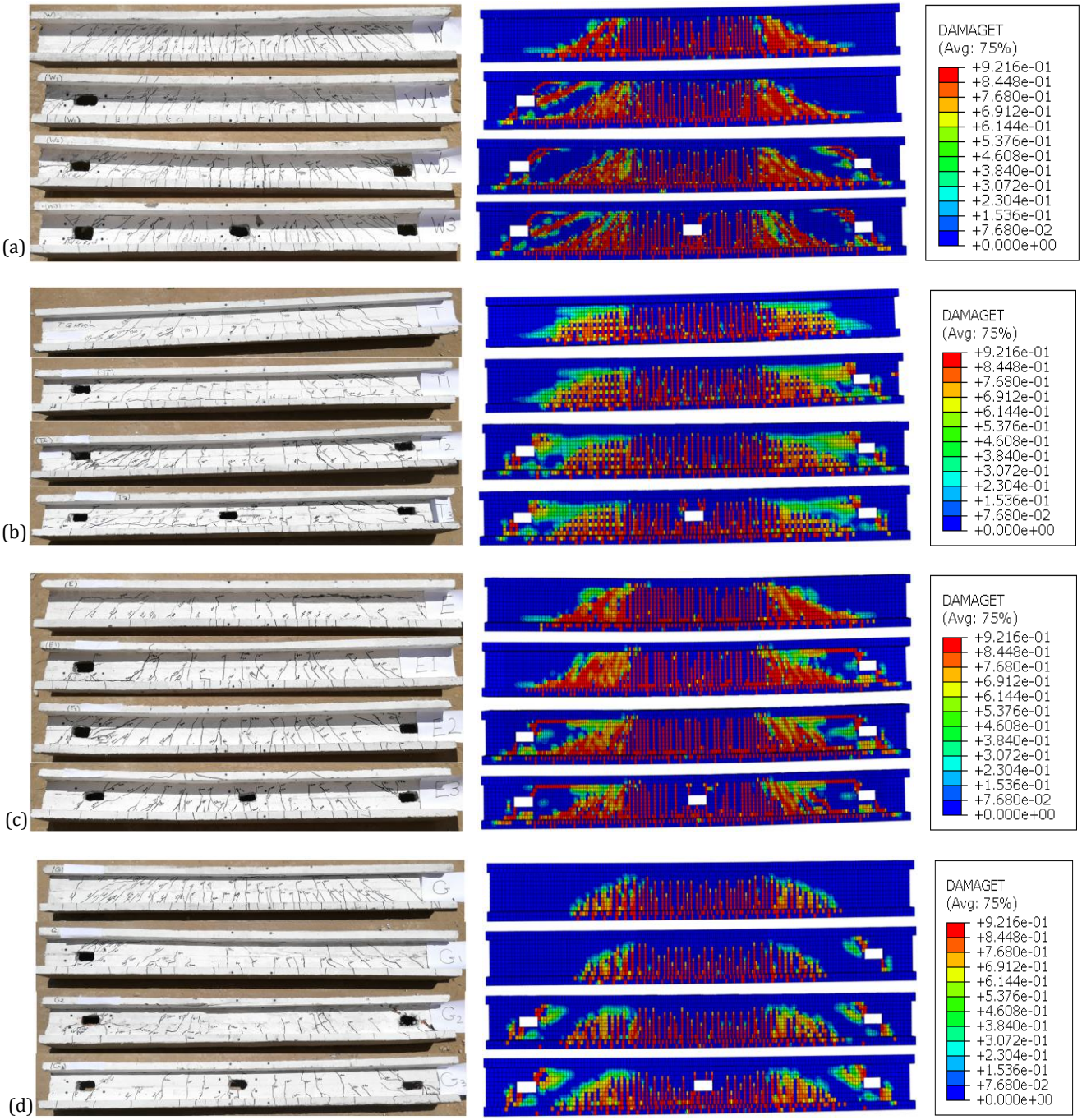

Fig. 23. Experimental and F.E. crack pattern of the tested beams: (a) Group A; (b) Group B; (c) Group C; (d) Group D.

A three-dimensional finite element model was developed, taking into account the nonlinear material behavior of the reinforcing metal mesh and concrete. The model was validated using the experimental test results and showed good agreement.

The results showed that beams with no openings, one, and two openings reinforced with Gavazzi meshes had the highest ultimate load compared to other tested beams, while beams with three openings, those reinforced with expanded metal meshes had the greatest ultimate loads. Placing three openings in beams, with dimensions of 100×50 mm (two of these openings are approximately 10 cm apart from each edge while the third opening is located at mid-span), reduced the load-to-weight ratio by about 20.7%, 12.9%, 8.2%, and 23.8% for welded beams, expanded beams, Tensar beams, and Gavazzi beams, respectively, compared to the beams with no openings.

Based on the experimental and FE results available, the following conclusions can be drawn:

- The efficiency of beams is negatively affected by the presence of openings, resulting in a decrease of ultimate loads by approximately 5.2%, 10.5%, and 15.6% on average for one, two, or three openings, respectively, compared to beams without openings.
- In the case of beams with one, two, and three openings, the utilization of expanded metal meshes resulted in a higher ductility ratio and energy absorption capacity compared to other tested mesh types. However, for beams with no openings, the use of

welded steel meshes demonstrated greater ductility and energy absorption while also potentially leading to increased deflection values.

- When considering beams with three openings, the use of expanded metal meshes resulted in a higher ultimate load capacity compared to beams with welded steel meshes, beams with Tensar meshes, and beams with Gavazzi meshes by 4%, 14.8%, and 4.2%, respectively. Moreover, the placement of three openings in such beams decreased the load-to-weight ratio by 20.7%, 12.9%, 8.2%, and 23.8% in welded beams, expanded beams, Tensar beams, and Gavazzi beams, respectively, compared to beams with no openings.
- The deflection values for beams with one, two, and three openings varied depending on the type of reinforcement used. In particular, for beams with one opening, beam E1 had a higher deflection value compared to beams W1, T1, and G1, with deflection increases of 3.3%, 61.2%, and 56.1%, respectively. For beams with two openings, beam E2 showed a higher deflection value compared to beams W2, T2, and G2, with deflection increases of 6.1%, 77.8%, and 62.5%, respectively. Similarly, for beams with three openings, beam E3 demonstrated a higher deflection value compared to beams W3, T3, and G3, with deflection increases of 12.7%, 82.0%, and 71.9%, respectively.
- For the welded steel meshes group, beam W3 demonstrated a lower deflection value than beam W0 by 25.3%, while for the expanded metal meshes group, beam E3 showed a lower deflection value than beam E0 by 13.1%. Beams with welded steel meshes had a higher deflection than the other tested beams for beams without openings, while for beams with one, two, and three openings, beams with expanded metal meshes had a higher deflection than the other tested beams.
- For the Gavazzi meshes group, beam G3 exhibited a lower deflection value than beam G0 by 18.2%, while for the Tensar meshes group, beam T3 demonstrated a lower deflection value than beam T0 by 18.7%.
- Beams with Gavazzi meshes demonstrated a higher ultimate load capacity than beams with Tensar meshes by 23.2%, 21.3%, 15.6%, and 10.2% for beams without openings, one, two, and three openings, respectively. However, the ultimate load capacity in beams with three openings decreased by 21.4% compared to the ultimate load capacity in beams with no openings for Gavazzi mesh beams, whereas it decreased by 12.2% for Tensar mesh beams.
- For beams with no opening, one and two openings, Gavazzi mesh beams exhibited a greater ultimate load than the other tested beams, while for beams with three openings, expanded metal mesh beams demonstrated the greatest ultimate loads. Furthermore, Gavazzi mesh beams showed a higher ultimate load than welded steel mesh beams by 3.8%, 8.6%, and 3.9% for beams without opening, one and two openings, respectively, whereas Gavazzi mesh beams displayed a higher ultimate load than expanded metal mesh beams by 9.2%, 10.1%, and 2.5% for beams without opening, one and two openings, respectively.

Acknowledgements

None declared.

Funding

The authors received no financial support for the research, authorship, and/or publication of this manuscript.

Conflict of Interest

The authors declared no potential conflicts of interest with respect to the research, authorship, and/or publication of this manuscript.

Author Contributions

All of the authors made substantial contributions to conception and design, or acquisition of data, or analysis and interpretation of data; were involved in drafting the manuscript or revising it critically for important intellectual content; and gave final approval of the version to be published.

Data Availability

The datasets created and/or analyzed during the current study are not publicly available, but are available from the corresponding author upon reasonable request.

REFERENCES

Abaqus Documentation User's Guide (2014). Dassault Systemes, Simulia Corp, Providence, USA.

ACI 5492R (2004). Report on thin reinforced cementitious products. American Concrete Institute, Farmington Hills, Michigan, USA.

ACI 549R (1997). State of the art report on ferrocement, Manual of concrete practice. American Concrete Institute, Farmington Hills, Michigan, USA.

Acma LMC, Dumpasan GC, Salva MI, Mansaguiton MP, Supremo RP, Daquiado NFP (2015). Flexural strength and ductility behavior of ferrocement i-beam. Mindanao Journal of Science and Technology, 13, 99-108.

Acma LMC, Mariano C (2014). Development and Application of Ferrocement I-beams. *Ph.D. thesis*, Mindanao State University - Iligan Institute of Technology, Iligan City, Philippines.

Ankit B, Sumit G, Lalit K, Hardik S (2017). A review study of application of ferrocement. *International Research Journal of Engineering and Technology*, 4(6), 1592-1597.

Austriaco RL (2006). Research and innovations on ferrocement in the new millenium: global perspective. *Proceedings of 8th International Symposium and Workshop on Ferrocement and Thin Reinforced Cement Composites*, Thailand, IFS, 77-86.

ChandraSekharRao T, GunneswaraRao TD, RamanaRao NV, Rambabu C (2012). An experimental study on ferrocement box-beams under flexural loading. *International Journal of Emerging Technology and Advanced Engineering*, 2(9), 2250-2459.

E.S.S. 262 (2011). Egyptian standard specifications for steel bars. Ministry of Industry, Cairo, Egypt.

Hekal GM, Salama MI, Elsamak G, Almaadawy AH (2023). Shear behavior of RC beams strengthened with ultra-high-performance fiber-reinforced concrete using finite-element analysis. *Asian Journal of Civil Engineering*, 24, 71–91.

International Ferrocement Society (2001). Ferrocement model code. Thailand, IFS.

Naaman AE (2000). Ferrocement and Laminated Cementitious Composites. Techno-Press 3000, Ann Arbor, Michigan, USA.

Pathak A (2020). Effect of silica fume and fly ash as partial replacement of cement on strength of concrete. *International Conference of Advance Research & Innovatio*, India, 167-170.

Rameshkumar M, Malathy R, Chandiran P, Paramasivam S, Chung IM, Kim SH, Prabakaran M (2022). Study on flexural behaviour of ferrocement composites reinforced with polypropylene warp knitted fabric. *Polymers*, 14(19), 4093.

Safiuddin MD, Zain MFM (2005). Effects of silica fume and fly ash on the properties of high-performance concrete. *Proceedings of the Annual Conference on Canadian Society for Civil Engineering*, Toronto, Canada, 2-4.

Salman WD, Mubarak HM, Mahmood MS (2018). Structural behavior and mechanical properties of ferrocement slab panels incorporating fibers. *International Journal of Civil Engineering and Technology (IJCIET)*, 9(11), 2289-2298.

Shaaban IG, Shaheen YBI, Elsayed EL, Kamal OA, Adesina PA (2018). Flexural behaviour and theoretical prediction of lightweight ferrocement composite beams**.** *Case Studies in Construction Materials*, 9, e00204.

Shaheen YBI, Mohamed AM, Mohamed HR (2016). Structural performance of ribbed ferrocement plates reinforced with composite materials. *Structural Engineering and Mechanics*, 60(4), 567-594.

Shaheen YBI, Mousa M, Gamal E (2020), Structural behavior of lightweight ferrocement walls. *13th International Conference on Civil and Architecture Engineering*, Cairo, Egypt, 1-21.

Shaheen YBI, Eid FM, Mesalam O (2021). Structural behavior of ferrocement concrete plates subjected to flexural and dynamic loadings. *Journal of Engineering Research and Reports*, 21(7), 71-84.

Shaheen YBI, Etman ZA, Elrefy AM (2022a). Structural behavior of ferrocement composite hollow-cored panels for roof construction. *Challenge Journal of Concrete Research Letters*, 13(1), 5-27.

Shaheen YBI, Hekal GM, El Shaboury AM (2022b). Structural behavior of ferrocement I-beams with web openings – experimental study. *Engineering Research Journal, Menoufia University*, 45(4), 581-589.

Shaheen YBI, Etman ZA, Kandil DEA (2023a). Performance of light weight ferrocement composite walls. *Challenge Journal of Concrete Research Letters*, 14(3), 69-88.

Shaheen YBI, Hekal GM, Fadel AK (2023b). Structural behavior of multi-cell ferrocement composite beams. *International Conference on Advances in Structural and Geotechnical Engineering*, Hurghada, Egypt, 1-17.

Sumadi S, Ramli M (2008). Development of Lightweight Ferrocement Sandwich Panels for Modular Housing and Industrialized Building System. Project Report, University Teknologi Malaysia (UTM), Research Vote 73311, Johor, Malaysia.

Suresh V (2004). Application of ferrocement for cost-effective building construction. *Journal of Ferrocement*, 34(4), 445-455.